Big bang nucleosynthesis and early dark energy in light of the EMPRESS Y_p results and the H_0 tension

Tomo Takahashi [1] and Sora Yamashita [2]

[1] *Department of Physics, Saga University, Saga 840-8502, Japan*
[2] *Graduate School of Science and Engineering, Saga University, Saga 840-8502, Japan*

(Received 16 November 2022; accepted 3 April 2023; published 16 May 2023)

Recent measurements of the primordial ^{4}He abundance Y_p from EMPRESS suggest a cosmological scenario with an effective number of neutrino species that deviates from the standard value and a nonzero lepton asymmetry. We argue that the standard cosmological model would be extended further if the Hubble tension were taken into account, in which the derived baryon density could be somewhat higher than the in the standard ΛCDM framework. We also discuss the issue by assuming early dark energy whose energy density can have a sizable fraction at the epoch of big bang nucleosynthesis. We show that the existence of early dark energy can reduce some of the tension implied by the EMPRESS Y_p results.

DOI: 10.1103/PhysRevD.107.103520

I. INTRODUCTION

The concordance model of cosmology—the so-called ΛCDM model—has now been established and can successfully explain various cosmological observations almost consistently. However, in recent years several tensions in the framework of ΛCDM have come under debate, which may suggest a modification/extension of the concordance ΛCDM model. One of them is the Hubble tension (the H_0 tension), i.e., the discrepancy in the values of the Hubble constant H_0 measured directly in the local Universe and indirectly from sources such as the cosmic microwave background (CMB) in the framework of ΛCDM. More specifically, the Cepheid-calibrated supernova distance ladder measurements give $H_0 = 73.04 \pm 1.04$ km/s/Mpc [1], while CMB data from *Planck* in combination with baryon acoustic oscillation (BAO) measurements infer $H_0 = 67.66 \pm 0.42$ km/s/Mpc [2], which are discrepant at the 4.8σ level. Even without CMB data, the tension between direct and indirect measurements still persists [3–5] and indeed other direct and indirect measurements also show a similar tendency for each category (see, e.g., Refs. [6,7] for a review), which has motivated many efforts to resolve the tension and pursue models beyond the standard ΛCDM (see, e.g., Refs. [6,8] for a review).

Another issue has appeared recently from the measurement of the primordial ^{4}He abundance Y_p by the Extremely Metal-Poor Representatives Explored by the Subaru Survey (EMPRESS) experiment, which obtained $Y_p = 0.2370^{+0.0033}_{-0.0034}$ [9]. This value is somewhat smaller than the previously obtained ones, such as $Y_p = 0.2449 \pm 0.0040$ [10], $Y_p = 0.2436^{+0.0039}_{-0.0040}$ [11], and $Y_p = 0.2462 \pm 0.0022$ [12]. Further confirmation of the value of Y_p measured by the EMPRESS may be awaited in investigating its implications to cosmological parameters, once we take the EMPRESS value of Y_p, by combining the measurement of the deuterium abundance D_p from Ref. [13], $D_p = (2.527 \pm 0.030) \times 10^{-5}$, one obtains constraints on the effective number of neutrino species $N_{\rm eff} = 2.37^{+0.19}_{-0.24}$ and the baryon-to-photon ratio $\eta \times 10^{10} = 5.80^{+0.13}_{-0.16}$ [9] in the framework of the $\Lambda\mathrm{CDM} + N_{\rm eff}$ model. The value of $N_{\rm eff}$ deviates from the standard one[1] and the baryon-to-photon ratio is slightly smaller than that obtained from *Planck* in the framework of the ΛCDM model. This may create another tension in the standard cosmological model, which is referred to as the "helium anomaly" in some literature.

Actually, when one introduces a nonzero chemical potential for the electron neutrino μ_{ν_e}, which is commonly characterized by the degeneracy parameter $\xi_e = \mu_{\nu_e}/T$, with T being the neutrino temperature, one obtains $\xi_e = 0.05^{+0.03}_{-0.02}$ and $N_{\rm eff} = 3.11^{+0.34}_{-0.31}$ [9] with a Gaussian prior for the baryon-to-photon ratio $\eta \times 10^{10} = 6.132 \pm 0.038$ motivated by the *Planck* result in the ΛCDM framework [2].[2] This suggests a nonzero lepton asymmetry, and its implications have been discussed in Refs. [21–24]. Instead of invoking a nonzero lepton asymmetry, one can also envisage a model with modified gravity [25] to resolve the helium anomaly. In any case, the EMPRESS result may indicate that we need a model beyond the standard paradigm and it would raise another tension in cosmology.

[1] Although we use $N_{\rm eff} = 3.046$ [14] as a reference value for the standard case, recent precise calculations gave $N_{\rm eff} =$ 3.044–3.045 [15–19].

[2] See Ref. [20] for the implications of a nonzero lepton asymmetry and extra radiation for the H_0 tension.

TABLE I. Constraints on the baryon density $\Omega_b h^2$ and its corresponding baryon-to-photon ratio η_{10} in models proposed to resolve the H_0 tension. For the data set shown in the fifth column, (a)–(f) denotes: (a) *Planck* 2018 + BAO, (b) *Planck* 2018 + BAO + Supernova (SN) + H_0, (c) *Planck* 2018 + BAO + SN + H_0 + RSD + DES, (d) *Planck* 2018 + BAO + SN + BBN + H_0, (e) *Planck* 2018 + SN + H_0, and (f) *Planck* 2018 + BAO + SN + DES + H_0. Here "*Planck* 2018" refers to *Planck* 2018 TT, TE, EE + lensing, and "H_0" indicates that the analysis adopts the H_0 prior with the value motivated by a direct local measurement such as the one from distance ladder observations. For details of the analysis, see the references shown in the last column. We should note that most analyses quoted in the table include the H_0 prior, and hence some caution should be taken when interpreting the value of H_0 obtained in the analyses.

Model	$100\Omega_b h^2$	η_{10}	H_0	Data set	Ref.
ΛCDM	2.242 ± 0.014	6.14 ± 0.038	67.66 ± 0.42	(a)	[2]
Varying $m_e + \Omega_k$	$2.365^{+0.033}_{-0.037}$	$6.48^{+0.090}_{-0.101}$	$72.84^{+1.0}_{-1.0}$	(b)	[33]
Early dark energy (ϕ^4 + AdS)	$2.346^{+0.017}_{-0.016}$	$6.42^{+0.047}_{-0.044}$	$72.64^{+0.57}_{-0.64}$	(b)	[34]
Early dark energy (axion type)	2.285 ± 0.021	6.26 ± 0.057	$70.75^{+1.05}_{-1.09}$	(c)	[35]
New early dark energy	$2.292^{+0.022}_{-0.024}$	$6.27^{+0.060}_{-0.066}$	$71.4^{+1.0}_{-1.0}$	(d)	[36]
Early modified gravity	2.275 ± 0.018	6.23 ± 0.049	71.21 ± 0.93	(e)	[37]
Primordial magnetic field	2.266 ± 0.014	6.20 ± 0.038	70.57 ± 0.61	(f)	[38]
Majoron	2.267 ± 0.017	6.21 ± 0.047	70.18 ± 0.61	(a)	[39]

Actually, as we will argue in this paper, when the Hubble tension is taken into account the above EMPRESS result would imply a nonstandard scenario even more. In many attempts to explain the H_0 tension, it can be resolved in such a way that the value of H_0 derived indirectly from, e.g., CMB and BAO data increases and becomes similar to that from direct measurements. Indeed, the baryon density obtained in such model frameworks tends to be higher than the value in the ΛCDM case, which makes the above-mentioned discrepancy more severe. We discuss this issue quantitatively by investigating the fit to the EMPRESS Y_p result in combination with deuterium abundance from recent observations compiled by the Particle Data Group [26], $D_p = (2.547 \pm 0.025) \times 10^{-5}$,[3] with the prior for the baryon density suggested by the H_0 tension.

Moreover, we also argue that one can reduce the helium anomaly by extending the standard cosmological model with an extra component called early dark energy (EDE) [27] which has been extensively discussed in the context of the H_0 tension (for various works on EDE, see, e.g., Ref. [6]). Although the EDE model we consider in this paper has a different energy scale than the one introduced to resolve the H_0 tension, the behavior is quite similar in the sense that the energy density of EDE gives a sizable contribution to the total one during the epoch of big bang nucleosynthesis (BBN). Indeed, as we discuss in this paper, we do not need to assume nonzero lepton asymmetry or a nonstandard value of $N_{\rm eff}$ by assuming the existence of EDE in some cases to relax the helium anomaly.

The structure of this paper is as follows. In the next section, we discuss the implications of the Hubble tension for BBN, particularly focusing on its consequences for the EMPRESS Y_p results through the value of the baryon density suggested by models that may resolve the H_0 tension. Then, in Sec. III we argue that, by introducing EDE whose energy fraction becomes relatively large during the BBN era, the anomaly implied by the EMPRESS results can be alleviated. In the final section, we conclude our paper.

II. IMPLICATIONS OF THE HUBBLE TENSION FOR BBN

In this section, we discuss the implication of the H_0 tension for BBN, especially focusing on the effects of the assumption of baryon density suggested by the tension on the parameter estimation in BBN. In Table I we list the constraints on the baryon density $\Omega_b h^2$ in the ΛCDM model and example models proposed to resolve the H_0 tension. Most models in the list are taken from among those referred to as "successful" models as a possible solution to the H_0 tension in Ref. [8] based on the criteria of the Gaussian tension, the difference of the maximum *a posteriori* and the Akaike information criterium (see Table 1 in Ref. [8]). We take the constraints on $\Omega_b h^2$ from the references cited in the last column of Table I. We should note that the data set used in the analysis for each model quoted in Table I are different, and currently there is no consensus on which model is more plausible, and hence the values quoted in the table can be regarded as just a reference. Nevertheless, we can clearly see that, in models proposed as a solution to the H_0 tension, the value of $\Omega_b h^2$ tends to be higher than that in the ΛCDM model, which shows that the H_0 tension affects another aspect of cosmology.[4]

[3] In Ref. [9], the deuterium abundance obtained in Ref. [13] was adopted in the analysis, while we use the one given in Ref. [26] in our analysis. We note that the use of either value scarcely affects our argument.

[4] Other implications of the H_0 tension for other aspects of cosmology have been discussed, such as cosmological bounds on neutrino masses [28] and the scale dependence of the primordial power spectrum [29–32].

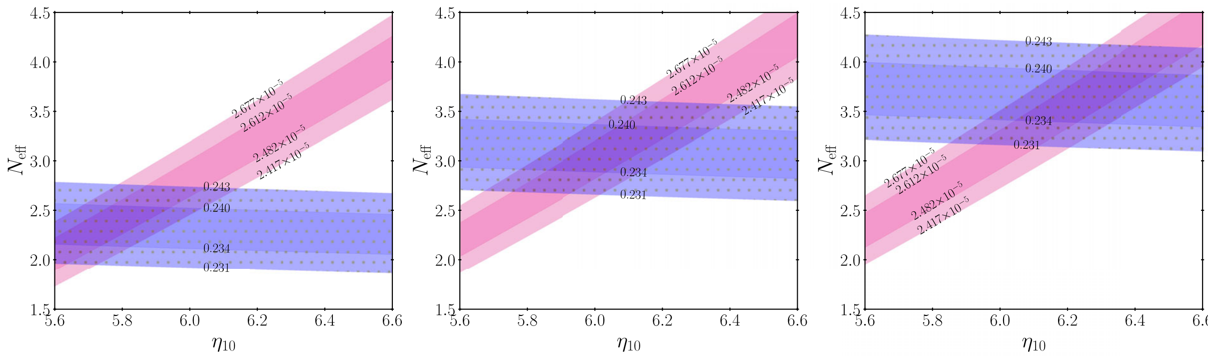

FIG. 1. Parameter ranges within 1σ and 2σ errors for Y_p [9] (light and dark dotted (blue) regions) and D_p [26] (light and dark magenta regions for 1σ and 2σ) in the η_{10}-$N_{\rm eff}$ plane. Here the 1σ and 2σ errors include both observational and theoretical ones. We take the neutrino degeneracy parameter as $\xi_e = 0$ (left), 0.05 (middle), and 0.08 (right).

Actually, this is somewhat expected given the correlation between $\Omega_b h^2$ and H_0 in the position and height of acoustic oscillations in the CMB angular power spectrum (see, e.g., Refs. [40,41]), although it becomes somewhat involved in models where the H_0 tension can be solved. To resolve the tension, one needs to reduce the sound horizon at recombination, r_s, but also keep the CMB angular power spectra almost intact to obtain a good fit to CMB (and BAO) data. For example, in the time-varying electron mass model [33], one can reduce r_s by slightly raising the electron mass m_e at the recombination epoch; however, to keep a good fit to CMB data, the baryon density $\Omega_b h^2$ should also be increased in accordance with the change of m_e as $\delta m_e/m_e = \delta(\Omega_b h^2)/\Omega_b h^2$ (see Ref. [33] for a detailed discussion). Also in the early dark energy model, in order to increase the value of H_0, one needs to shift $\Omega_b h^2$ to a higher value to have the CMB angular power spectrum almost the same, which can be realized by keeping the acoustic scale and angular damping scale almost unchanged (for details, see, e.g., Ref. [29]).

When one discusses BBN, the baryon density is usually quoted by the baryon-to-photon ratio $\eta = n_b/n_\gamma$, with n_b and n_γ being the number densities of baryons and photons, respectively. The conversion factor from the baryon density $\Omega_b h^2$ to the baryon-to-photon ratio $\eta_{10} = 10^{10}\eta$ is given by [42] (see also, e.g., Refs. [43,44])

$$\eta_{10} = \frac{273.279}{1 - 0.007125 Y_p}\left(\frac{2.7255\ \mathrm{K}}{T_{\gamma 0}}\right)^3 \Omega_b h^2, \quad (2.1)$$

where $T_{\gamma 0}$ is the present photon temperature. Precisely speaking, the conversion factor depends on the primordial helium abundance. Although we adopt the EMPRESS mean value of $Y_p = 0.2379$ to obtain η_{10}, the dependence on Y_p is very weak and thus its uncertainty can be neglected compared to the error in $\Omega_b h^2$ obtained from CMB data, and hence the actual value of Y_p in Eq. (2.1) scarcely affects the following argument. We also list the value of η_{10} derived by using Eq. (2.1) for each model in Table I. As seen from the table, models proposed to resolve the H_0 tension tend to suggest a higher value of η_{10} compared to that in ΛCDM. In some cases, the mean value of η_{10} can be as high as $\eta_{10} \sim 6.48$, although, in general, the error is also somewhat larger than that for the ΛCDM case.

Indeed, as already argued in Ref. [9], the value of Y_p obtained by EMPRESS would imply a nonzero lepton asymmetry, which is characterized by a nonzero electron neutrino degeneracy parameter ξ_e, and the value of $N_{\rm eff}$ is somewhat larger than the standard one. This tendency becomes more prominent when the baryon density is high, which can be understood from Fig. 1 where the 1σ and 2σ allowed regions from the measurements of Y_p [9] and D_p [26] are shown in the η_{10}-$N_{\rm eff}$ plane for several values of ξ_e. The errors include both observational and theoretical ones. [For the uncertainties from theoretical calculations, see the paragraph below Eq. (2.2).] We use the public code PARTHENOPE [42,45,46] to calculate the helium and deuterium abundances. As seen from the figure, as ξ_e takes more positive values, Y_p decreases [47], which makes a higher η_{10} preferred from the combination of the EMPRESS Y_p results [9] and D_p from Ref. [26]. This indicates that when a higher value of the baryon density is favored from CMB data, which can be taken into account in the analysis as a prior for η_{10} (as will be done in the following), a more (positively) nonzero value of ξ_e and a $N_{\rm eff}$ higher than the standard value are preferred.

To discuss the implication of a high value of η_{10} suggested by the H_0 tension in a more quantitative manner, we investigate a constraint in the $N_{\rm eff}$-ξ_e plane from the helium abundance Y_p of EMPRESS [9] and deuterium D_p [26] with the prior for the baryon-to-photon ratio η_{10}. To obtain the constraint, we calculate χ^2 as

$$\chi^2 = \frac{(Y_p^{\rm obs} - Y_p^{\rm th})^2}{\sigma^2_{Y_p,\rm obs} + \sigma^2_{Y_p,\rm sys}} + \frac{(D_p^{\rm obs} - D_p^{\rm th})^2}{\sigma^2_{D_p,\rm obs} + \sigma^2_{D_p,\rm sys}} + \frac{(\eta_{10}^{\rm ref} - \eta_{10})^2}{\sigma^2_{\eta_{10}}}. \quad (2.2)$$

In our analysis, we adopt $Y_p^{\rm obs} = 0.2379$, $\sigma_{Y_p,{\rm obs}} = 0.00335$ for the helium abundance, which is obtained by EMPRESS [9]. For the deuterium abundance, we use the weighted mean of 11 recent measurements of D_p compiled by the Particle Data Group [26]: $D_p^{\rm obs} = 2.547 \times 10^{-5}$ $\sigma_{D_p,{\rm obs}} = 0.025 \times 10^{-5}$. We also include the errors in the theoretical calculation for helium as $\sigma^2_{Y_p,{\rm sys}} = (0.0003)^2 + (0.00012)^2$, where the first and second errors come from the uncertainties on the nuclear rate and neutron decay rate with $\tau_n = 879.4 \pm 0.6$ sec [48], respectively [46]. For deuterium, we adopt $\sigma^2_{D_p,{\rm sys}} = (0.06 \times 10^{-5})^2$ which comes from nuclear rate uncertainties [46]. $Y_p^{\rm th}$ and $D_p^{\rm th}$ are theoretically predicted values for given model parameters, such as $\eta_{10}, N_{\rm eff}$, and ξ_e. How the abundances $Y_p^{\rm th}$ and $D_p^{\rm th}$ depend on $\eta_{10}, N_{\rm eff}$, and ξ_e can be read off from some fitting formulas given in, e.g., Ref. [49]. When we vary the baryon density η_{10} in the analysis, we add the third term to determine the value of χ^2.

For the baryon density, we consider three priors motivated by the constraints from CMB analysis in the standard ΛCDM model and models proposed to solve the H_0 tension. We take the following reference values for $\eta_{10}^{\rm ref}$ and $\sigma_{\eta_{10}}$:

$$\eta_{10}^{\rm ref,1} = 6.14, \qquad \sigma_{\eta_{10},1} = 0.038, \tag{2.3}$$

$$\eta_{10}^{\rm ref,2} = 6.40, \qquad \sigma_{\eta_{10},2} = 0.060, \tag{2.4}$$

$$\eta_{10}^{\rm ref,3} = 6.25, \qquad \sigma_{\eta_{10},3} = 0.060. \tag{2.5}$$

For the reference value 1 (denoted as "ref,1"), which is motivated by the analysis in the standard ΛCDM framework, we take $\eta_{10}^{\rm ref,1}$ and $\sigma_{\eta_{10},1}$ to be the same as in the ΛCDM model in Table I.

For the reference values 2 and 3, we take the values motivated from the analysis which can resolve the H_0 tension. As seen from Table I, the mean value of η_{10} varies from model to model; however, one can see the tendency that a higher η_{10} is preferred when a model allows a higher value of H_0. In order for the value of H_0 from indirect measurements such as the CMB to be consistent with that obtained from direct measurements, it should be high enough to be close to $H_0 = 73.04 \pm 1.04\,{\rm km/s/Mpc}$ [1]. Among the values for H_0 listed in Table I, the ones in varying $m_e + \Omega_k$ and early dark energy (EDE: ϕ^4 + AdS) models are close to it, in which the mean values of the baryon density are $\eta_{10} = 6.48$ and 6.42, respectively. Furthermore, new dark energy models and early modified gravity can also give a relatively high value of H_0, although its values are not as high as the ones in the models above (varying $m_e + \Omega_k$ and EDE ϕ^4 + AdS). In those models, the mean baryon densities are $\eta_{10} = 6.27$ and 6.23 and are somewhat larger than the one in ΛCDM. Motivated by these observations, we consider two reference values of $\eta_{10} = 6.40$ and 6.25 ("ref, 2" and "ref, 3," respectively). The uncertainty of η_{10} in models to resolve the H_0 tension is somewhat larger than that in the ΛCDM case. Therefore, we take $\sigma_{\eta_{10},2} = \sigma_{\eta_{10},3} = 0.060$ for reference values 2 and 3, which corresponds to the average value for the uncertainty of η_{10} listed in Table I excluding ΛCDM (rounded up to the second decimal place).

In Fig. 2, we show the 1σ and 2σ allowed regions in the $N_{\rm eff}$-ξ_e plane obtained by evaluating χ^2 given in Eq. (2.2). From the figure, one can see that when a higher value of η_{10} is assumed for the prior, a more positively nonzero lepton asymmetry (nonzero degeneracy parameter for the electron

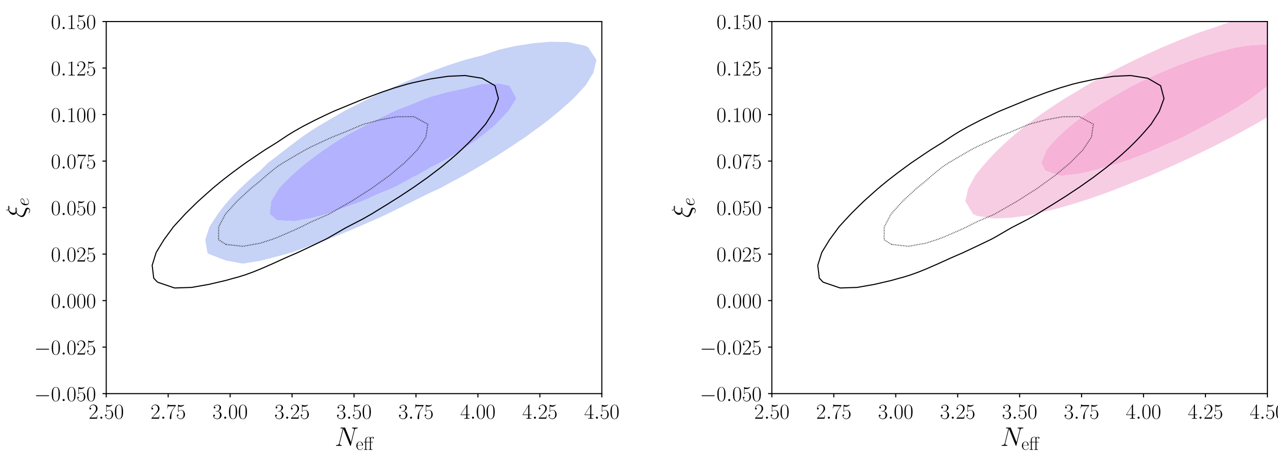

FIG. 2. 1σ and 2σ allowed regions in the $N_{\rm eff}$-ξ_e plane from measurements of Y_p and D_p with an η_{10} prior. For the η_{10} prior, we take $\eta_{10} = \eta_{10}^{\rm ref,1} \pm \sigma_{\eta_{10},1} = 6.14 \pm 0.038$ (black dotted and solid lines for 1σ and 2σ in both panels) obtained from CMB + BAO data [2] in the ΛCDM framework and $\eta_{10} = \eta_{10}^{\rm ref,2} \pm \sigma_{\eta_{10},2} = 6.4 \pm 0.060$ (light and dark shaded (magenta) regions for 1σ and 2σ in the right panel) and $\eta_{10} = \eta_{10}^{\rm ref,3} \pm \sigma_{\eta_{10},3} = 6.25 \pm 0.060$ (light and dark shaded (blue) regions for 1σ and 2σ in the left panel), which are suggested by the H_0 tension.

neutrino ξ_e) and larger value of $N_{\rm eff}$ are preferred, which indicates that, in light of the H_0 tension, the EMPRESS result for Y_p gives more significant effects on $N_{\rm eff}$ and the lepton asymmetry. (When a previous measurement of Y_p, such as from Refs. [10–12], is adopted, the allowed ranges for $N_{\rm eff}$ and ξ_e are closer to the standard ones compared to the case using the EMPRESS Y_p.)

In this section, we discussed the implications of a high baryon density, which may be suggested by the H_0 tension, for the EMPRESS Y_p results in the framework where a nonzero lepton asymmetry characterized by ξ_e and a nonstandard value of $N_{\rm eff}$ are allowed. Then, we showed that a positively large nonzero ξ_e and a larger $N_{\rm eff}$ than in the standard case are preferred. However, we can also consider another framework to discuss the implications of the EMPRESS Y_p results in light of the H_0 tension. As such an example, we will consider early dark energy model in the next section.

III. BIG BANG NUCLEOSYNTHESIS WITH EARLY DARK ENERGY

In this section we discuss the impact of EDE, which has been intensively studied in the context of the H_0 tension, on BBN in light of the EMPRESS result for Y_p. First we present the EDE model considered in this paper, and then we investigate constraints on $\eta_{10}, N_{\rm eff}$, and ξ_e from the EMPRESS Y_p in combination with the measurement of D_p for the case when EDE exists.

A. Early dark energy

EDE models have been extensively investigated in the context of the H_0 tension, whose typical realization is given by a scalar field ϕ with a potential, for example, such as $V(\phi) = V_0[1 - \cos(\phi/f)]^\alpha$ [50], with V_0 representing the energy scale, f being a parameter in the model, and α controlling the scaling of its energy density after ϕ starts to oscillate. A general behavior of the energy density of EDE, $\rho_{\rm EDE}$, is that when ϕ slowly rolls on the potential at early times, $\rho_{\rm EDE}$ is almost constant and acts like a cosmological constant, and then when the effective mass of ϕ becomes the same as the Hubble rate it starts to oscillate around the minimum of its potential. Around the minimum, the potential can be approximated as $V \propto \phi^{2\alpha}$ and hence its energy density scales as $\rho_{\rm EDE} \propto a^{-4}$ for $\alpha = 2$, $\rho_{\rm EDE} \propto a^{-9/2}$ for $\alpha = 3$, and so on. If EDE starts to oscillate around the epoch of recombination and has some energy fraction at the beginning of its oscillation, EDE affects the evolution of perturbations around recombination, and then soon becomes irrelevant to the evolution of the Universe since $\rho_{\rm EDE}$ dilutes away faster than matter, which is a scenario considered in the context of the H_0 tension. However, here we discuss a case where EDE can have a sizable energy density fraction at some time during BBN.

In the following, we consider two types of EDE. The first one is essentially the same as that adopted to resolve the H_0 tension [27], in which an EDE component behaves like a cosmological constant at early times, and then its energy density quickly dilutes away at some epoch during BBN. As mentioned above, the energy scale of EDE considered here is different from that motivated by the H_0 tension; such an EDE can be realized by assuming appropriate model parameters even for the same potential as that adopted to resolve the H_0 tension. One could also think of a scenario where two (or more) EDEs are embedded in one framework such as chain dark energy model [51] in which the Universe experiences multiple first-order phase transitions and some of them act as EDE at the BBN and recombination epochs. Another example of such models is cascading dark energy [52] where multiple scalar fields can act as dark energy during different eras, which can also accommodate a scenario where EDEs affect the epochs of recombination and BBN such that they relax both the H_0 tension and the helium anomaly.

Here we just assume an EDE which can have a sizable energy fraction during the BBN epoch, and then its energy density dilutes quickly, and we describe the evolution of its energy density by adopting the following phenomenological model for simplicity and generality such that the description can capture the essential behavior of the model. We model the evolution of the energy density of the first type of EDE, which we refer to as "EDE1" in the following, as

$$\rho_{\rm EDE1} = \begin{cases} \rho_0 & (T \geq T_t), \\ \rho_0 (\frac{T}{T_t})^n & (T < T_t), \end{cases} \tag{3.1}$$

where T is the cosmic temperature and T_t is the transition temperature at which the energy density changes its behavior. n is a parameter that describes the scaling of the energy density. Since the Universe is radiation-dominated during BBN, the temperature essentially scales as $T \propto 1 + z \propto 1/a$. ρ_0 is assumed to be constant, and hence it represents the vacuum energy before EDE starts to dilute away. We have modified the PARTHENOPE code [42,45,46] to include the EDE. In the calculation, we actually use the energy fraction of EDE at the time of transition, denoted as $f_{\rm EDE}$, to control the transition time instead of directly using T_t, which is defined by

$$f_{\rm EDE} \equiv \frac{\rho_{\rm EDE}(T_t)}{\rho_{\rm tot}(T_t)} = \frac{\rho_{\rm EDE}(T_t)}{\rho_{\rm EDE}(T_t) + \rho_{rB}(T_t)}, \tag{3.2}$$

where $\rho_{\rm tot}$ is the total energy density including the EDE component and $\rho_{rB}(T)$ is the sum of energy densities of photons, neutrinos, electrons, and baryons. In our calculation, we properly take account of the time variation of ρ_{rB} and set T_t for a given $f_{\rm EDE}$. One can approximately evaluate T_t for a given $f_{\rm EDE}$ as $T_t \sim 1\ {\rm MeV}((\rho_0/1\ {\rm MeV}^4)(1 - f_{\rm EDE}))^{1/4}$.

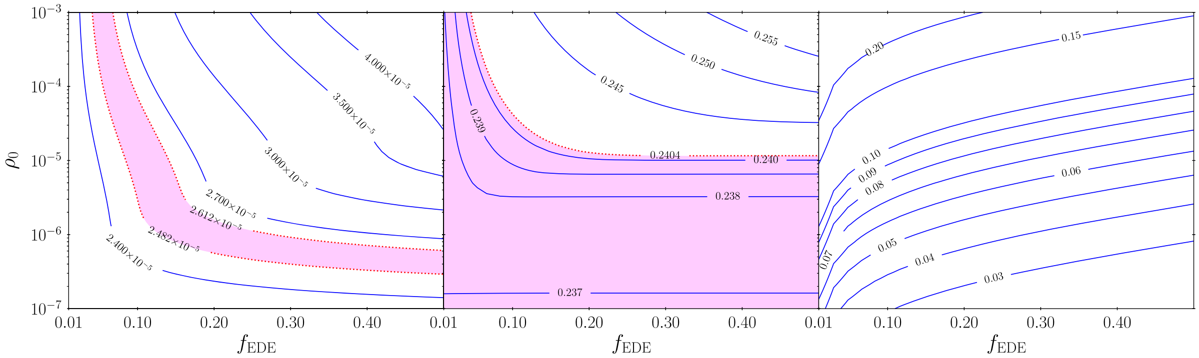

FIG. 3. Contours of D_p (left), Y_p (middle), and T_t [MeV] (right) in the $f_{\rm EDE}$-ρ_0 plane for EDE1 with $n = 4$. 1σ allowed ranges for Y_p and D_p, in which both observational and theoretical uncertainties are included, are lightly shaded (magenta). The value of ρ_0 is shown in units of MeV^4. In this figure, we take $\eta_{10} = 6.14$, $N_{\rm eff} = 2.3$, and $\xi_e = 0$.

Since ρ_{rB} monotonically decreases, but $\rho_{\rm EDE}$ is constant when $T > T_t$, the impact of EDE is the largest at around $T = T_t$.

The second type of EDE we consider is one that behaves as a negative cosmological constant until some time during BBN and it quickly settles down to the observed cosmological constant today. Although EDE with a negative energy density may be considered to be somewhat contrived or exotic, a negative cosmological constant has been investigated in the context of the H_0 tension [34,53,54] and the tension in BAO observations at $z \simeq 2.4$ between the ones observed from Lyman-α forest observations and the predicted values in the ΛCDM model[5] [59,60]. Furthermore, some theoretical frameworks motivate a negative dark energy such as bimetric gravity [61–63], graduated dark energy [64–66], ever-present Λ [67,68], and so on. In particular, in the ever-present Λ model, the energy fraction of negative dark energy can give a sizable contribution to the total one at some time due to its stochastic nature [67,68]. Although one could predict the evolution of such dark energy for a given model, here we assume that the EDE energy density changes from a negative constant to almost zero (actually, to a very small value which can explain the present-day dark energy) at some time during BBN. Since a tiny cosmological constant should be negligible compared to other energy components during the BBN epoch, to study the effect of this second type of EDE, which we refer to as "EDE2" in the following, we model the energy density of EDE2 simply as

$$\rho_{\rm EDE2} = \begin{cases} -\rho_0 & (T \geq T_t), \\ 0 & (T < T_t), \end{cases} \tag{3.3}$$

where ρ_0 is a constant, whose value represents the energy density of EDE2 at early times. As in the case of EDE1, instead of using T_t we in practice use the energy density fraction of EDE, $f_{\rm EDE}$, to specify the time when the transition from $\rho_{\rm EDE,2} = -\rho_0$ to $\rho_{\rm EDE,2} = 0$ occurs in our analysis. Since this kind of EDE can reduce the expansion rate of the Universe at some certain period during BBN, the study of this type of EDE also gives a general insight into models where the expansion rate diminishes at some particular epoch during BBN.

By assuming the two types of EDE described above, we discuss the impact of EDE on the abundance of light elements and its implications for the helium anomaly. In particular, we investigate constraints on the parameters such as $\eta_{10}, N_{\rm eff}$, and ξ_e in the presence of EDE to discuss its impact on BBN, which will be presented in the next section.

B. Impact of EDE on BBN

Here we discuss how the existence of EDE affects constraints on $\eta_{10}, N_{\rm eff}$, and ξ_e from the abundances of helium and deuterium, especially in light of the result from EMPRESS on Y_p and the H_0 tension.

First we show contours of D_p, Y_p, and T_t in the $f_{\rm EDE}$-ρ_0 plane for EDE1 with $n = 4$, 5 and 6 in Figs. 3, 4, and 5, respectively, where the other parameters are taken as $\eta_{10} = 6.14$, $N_{\rm eff} = 2.3$, and $\xi_e = 0$. The reason why we take $N_{\rm eff} = 2.3$, which is smaller than the standard value, is that when $N_{\rm eff} = 3.046$ and $\xi_e = 0$ are assumed, the value of Y_p is always larger than the 1σ upper limit obtained by EMPRESS in the ranges of $f_{\rm EDE}$ and ρ_0 shown in the figure, but by lowering the value of $N_{\rm eff}$, Y_p gets smaller so that the 1σ allowed range for Y_p becomes visible. Indeed, this value of $N_{\rm eff}$ is almost the same as the mean value for the standard case with $\xi_e = 0$ obtained in Ref. [9]. As seen from the figures, the dependences of Y_p on $f_{\rm EDE}$ and ρ_0 are almost the same for $n = 4$, 5, and 6; on the other hand, the contours for D_p behave differently for $n = 4$, 5, and 6, especially in the large-ρ_0 region. However, when one combines the data from Y_p and D_p, the allowed region becomes almost independent of n as shown in Fig. 7. Actually, the contours for T_t are the same for $n = 4$, 5,

[5] Although the tension has been suggested as $\sim 2\sigma$–2.5σ [55–57], it was reduced to 1.5σ in a recent measurement [58].

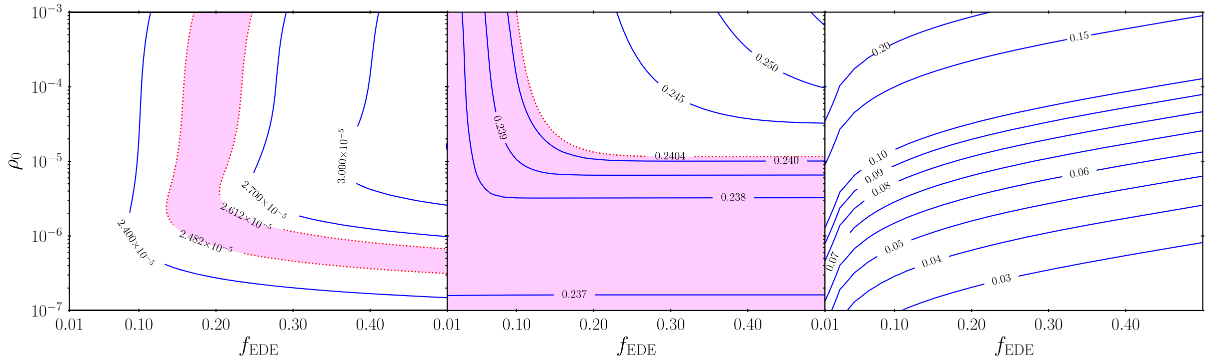

FIG. 4. The same as Fig. 3 except that $n = 5$ is assumed in this figure.

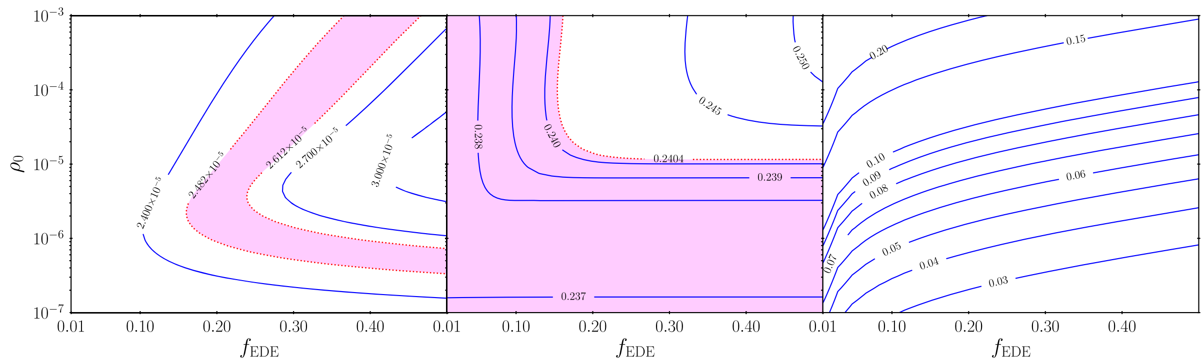

FIG. 5. The same as Fig. 3 except that $n = 6$ is assumed in this figure.

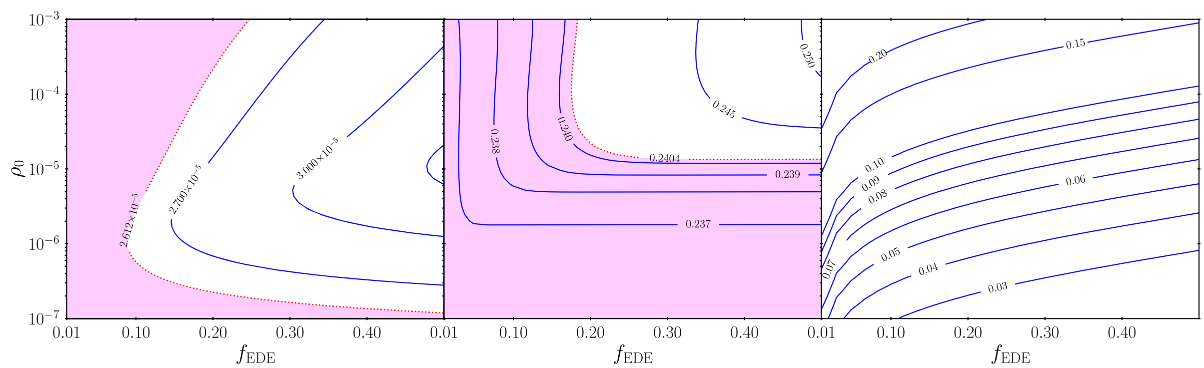

FIG. 6. The same as Fig. 3 except that $\eta_{10} = 5.80$ and $n = 6$ are assumed in this figure.

and 6 since T_t is the temperature when the energy density of EDE1 changes its behavior, which is irrelevant to the scaling of $\rho_{\rm EDE1}$ below $T = T_t$.

In Fig. 6, the case with $n = 6$ for $\eta_{10} = 5.80$, $N_{\rm eff} = 2.3$, and $\xi_e = 0$ is shown, which can be compared with Fig. 5 where $\eta_{10} = 6.14$ is assumed with other parameters to be the same as those in Fig. 5. Since $\eta_{10} = 5.80$ corresponds to the mean value for the standard case with $\xi_e = 0$ [9], regions with a smaller $f_{\rm EDE}$ are more widely allowed. By comparing Figs. 5 and 6, one can see that when η_{10} is large, the existence of EDE helps to improve the fit to Y_p and D_p.

When one assumes $n > 6$, the energy density of EDE dilutes faster than that for the cases presented here; however, we can expect that the allowed range from the combination of the data on Y_p and D_p will be almost unchanged as the cases for $n = 4$, 5, and 6 give the same results. On the other hand, in the case of $n < 4$, the energy density of EDE decreases slower than radiation and eventually dominates the Universe. Such an energy component would affect CMB anisotropies, which can easily exclude the model, and hence we do not consider such a case.

Since the existence of EDE affects the abundance of light elements through the change of the expansion rate of the Universe, in which the freeze-out time of nuclear reactions gets modified, the abundances of helium and deuterium

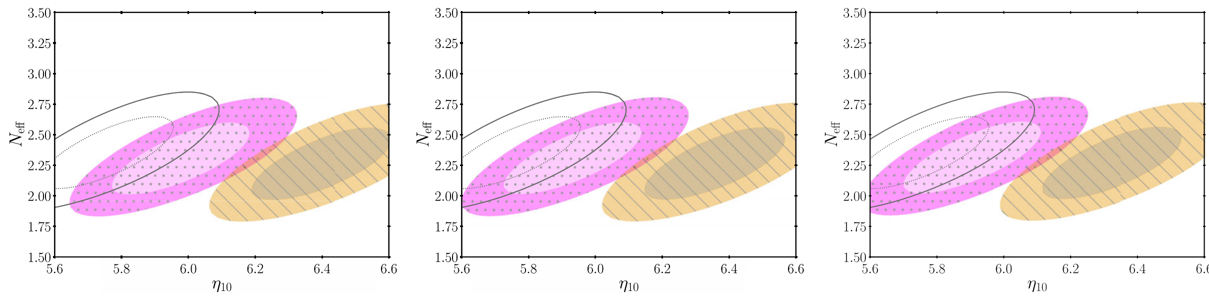

FIG. 7. 1σ and 2σ allowed regions in the η_{10}-$N_{\rm eff}$ plane from measurements of Y_p and D_p for EDE1 with $n = 4$ (left), 5 (middle), and 6 (right). We take $\rho_0 = 10^{-6}$ MeV^4 and $f_{\rm EDE} = 0.09$ (light and dark dotted (magenta) for 1σ and 2σ regions) and 0.50 (dark and light striped (orange) for 1σ and 2σ regions) in all panels. For reference, we also show the constraint for the case without EDE with black dotted (1σ) and solid (2σ) lines. In this figure, we assume no lepton asymmetry (i.e., $\xi_e = 0$).

change depending on $f_{\rm EDE}$ and ρ_0. As $f_{\rm EDE}$ or ρ_0 increases (i.e., the effects of EDE become larger), the expansion rate gets bigger, particularly around $T = T_t$, which makes the neutron freeze-out occur earlier and hence the value of Y_p increases. The same tendency also holds true for deuterium, which can be seen from the left panel of the figure. It should also be noticed that, in the bottom half region of the middle panel, Y_p scarcely changes even when $f_{\rm EDE}$ is increased. Indeed, this region corresponds to the one where the transition temperature is lower than 0.07 MeV, as seen from the right panel of the figure. Around this temperature, the helium abundance almost freezes out, below which the value of Y_p would not be affected even if the expansion rate is changed, i.e., the amount of EDE is irrelevant below $T_t \sim 0.07$ MeV. This is the reason why Y_p almost stays constant regardless of the change of $f_{\rm EDE}$. Compared to Y_p, since the deuterium abundance evolves gradually and does not reach a constant value until late times, D_p decreases continuously against the changes of $f_{\rm EDE}$ and ρ_0 although the response becomes insensitive in the bottom region, as in the case of Y_p.

As mentioned above, the cases of $n = 4$, 5, and 6 show almost the same tendency for Y_p; however, some differences appear for D_p in the region above $\rho_0 \gtrsim \mathcal{O}(10^{-6})$ MeV^4. Since the scaling of the energy density of EDE1 in the $n = 4$ case is the same as that of radiation, it mimics the effects of $N_{\rm eff}$ below $T = T_t$; on the other hand, when $n = 6$, $\rho_{\rm EDE}$ quickly dilutes away and EDE scarcely affect the expansion rate any more. Therefore, the difference between the cases with $n = 4$ and 6 only appears when EDE1 makes a contribution sufficient enough to affect the Hubble expansion rate even for $T < T_t$. (The case of $n = 5$ shows a behavior that is somewhat in between those of $n = 4$ and $n = 6$.) However, the allowed overlapping regions between Y_p and D_p are almost the same for the $n = 4$, 5, and 6 cases, and the final constraint is also virtually the same. To show this explicitly, we depict constraints from Y_p and D_p in the η_{10}-$N_{\rm eff}$ plane for the cases of $n = 4$, 5, and 6 in Fig. 7. In the figure, no lepton asymmetry is assumed (i.e., $\xi_e = 0$). We fix the value of ρ_0 as $\rho_0 = 10^{-6}$ MeV^4, whose value gives a good fit to the data, as shown in Fig. 9. Furthermore, we take two values for $f_{\rm EDE}$ as $f_{\rm EDE} = 0.09$ and 0.5 to show how the constraint depends on $f_{\rm EDE}$. As seen from the figure, regardless of the choice of the EDE parameters such as ρ_0 and $f_{\rm EDE}$, the constraints are virtually unchanged even if we assume a different value for n when both Y_p and D_p are taken into account. Therefore, we only consider the case of $n = 6$ for EDE1 in the rest of this paper. We should also mention that since the energy density of EDE1 with $n = 6$ dilutes faster than radiation and becomes negligible just below $T = T_t$, and hence it does not affect the later evolution of the Universe, such an EDE would affect the evolution of the Universe only during the BBN epoch.

Next, in Fig. 8 we show contours of Y_p and D_p for the case of EDE2 in the $f_{\rm EDE}$-ρ_0 plane. Here we take $\eta_{10} = 6.14$ and $\xi_e = 0$ as in Figs. 3–5, but we take $N_{\rm eff} = 3.046$ for this case. Since EDE2 gives a negative contribution to the total energy density of the Universe, which slows down the Hubble expansion rate, the responses of Y_p and D_p to the changes of $f_{\rm EDE}$ and ρ_0 show an opposite tendency to those in the case of EDE1, i.e., as $f_{\rm EDE}$ and/or ρ_0 increase, the values of Y_p and D_p decrease. However, as in the EDE1 case, the value of Y_p is almost unchanged near the bottom right region of the middle panel where the transition temperature is $T_t \lesssim 0.07$ MeV. As mentioned above, the helium abundance is almost fixed at this temperature, and hence the change of the expansion rate does not affect the final value of Y_p when $T_t < 0.07$ MeV, which is the reason why Y_p stays almost the same as $f_{\rm EDE}$ increases.

Now we are going to discuss the effects of EDE in combination with $N_{\rm eff}$. We show the allowed ranges from the Y_p and D_p measurements separately in the $f_{\rm EDE}$-$N_{\rm eff}$ plane in Figs. 9 and 10 for the cases of EDE1 and EDE2, respectively. The 1σ and 2σ regions, in which both observational and theoretical uncertainties are included, are depicted. In the figures, we fix the baryon density to $\eta_{10}^{\rm ref,1}$, $\eta_{10}^{\rm ref,2}$, and $\eta_{10}^{\rm ref,3}$ as shown in the plots, and take

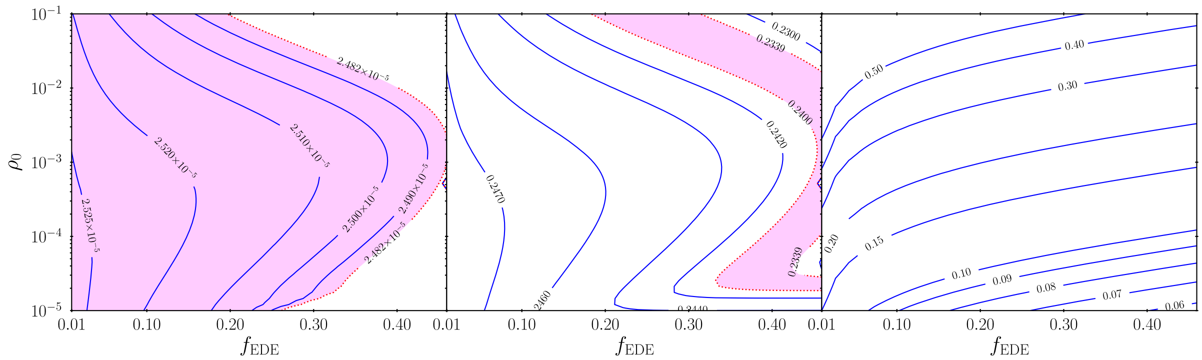

FIG. 8. Contours of D_p (left), Y_p (middle), and T_t [MeV] (right) in the f_{EDE}-ρ_0 plane for EDE2. The 1σ allowed region for Y_p and D_p is shown with light shade (magenta). The value of ρ_0 is shown in units of MeV^4. In this figure, we take $\eta_{10} = 6.14$, $N_{\mathrm{eff}} = 3.046$, and $\xi_e = 0$.

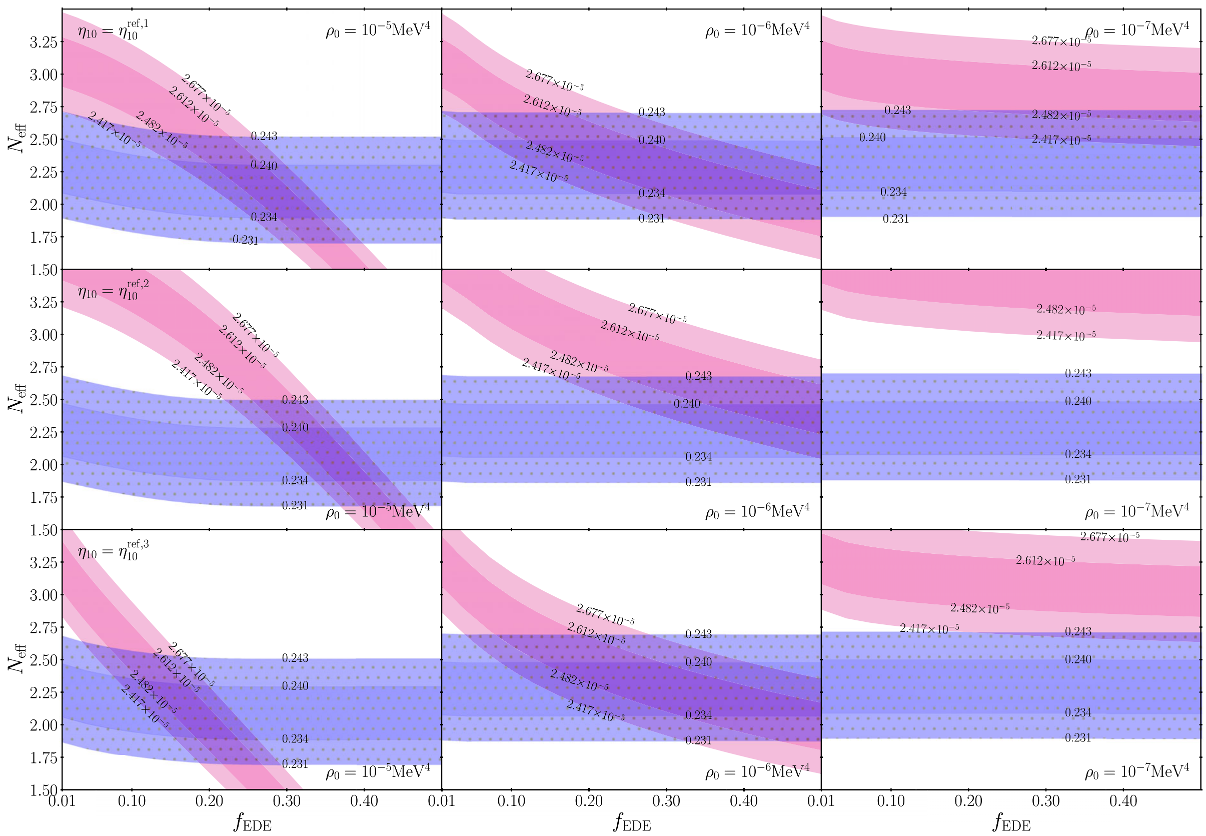

FIG. 9. 1σ and 2σ allowed ranges from observations of Y_p [9] (light and dark dotted (blue)) and D_p [26] (light and dark shaded (magenta)) in the f_{EDE}-N_{eff} plane for EDE1 with $n = 6$. The priors for η_{10} assumed in the analysis are $\eta_{10} = \eta_{10}^{\mathrm{ref},1}$ (top), $\eta_{10}^{\mathrm{ref},2}$ (middle), and $\eta_{10}^{\mathrm{ref},3}$ (bottom), as shown in the figure. The value of ρ_0 is fixed and is also shown in the figure. In all panels, the electron neutrino degeneracy parameter is fixed as $\xi_e = 0$.

several values for ρ_0 which are also indicated in the figure. In all cases, we take the electron neutrino degeneracy parameter as $\xi_e = 0$. From the figure, one can notice that when there is no EDE (i.e., when $f_{\mathrm{EDE}} \to 0$), there is almost no overlapping region between the allowed ones from the Y_p and D_p measurements in all cases for both EDE1 and EDE2. This is because, as seen from Fig. 1, the allowed regions from Y_p and D_p overlap at $\eta_{10} \sim 5.8$ in the η_{10}-N_{eff} plane when $\xi_e = 0$, but here we fix η_{10} to $\eta_{10}^{\mathrm{ref},1}$, $\eta_{10}^{\mathrm{ref},2}$, and $\eta_{10}^{\mathrm{ref},3}$, which are larger than $\eta_{10} \sim 5.8$. However, as f_{EDE} increases, the overlapping region between the ones allowed by Y_p and D_p measurements appears, which indicates that EDE can improve the fit.

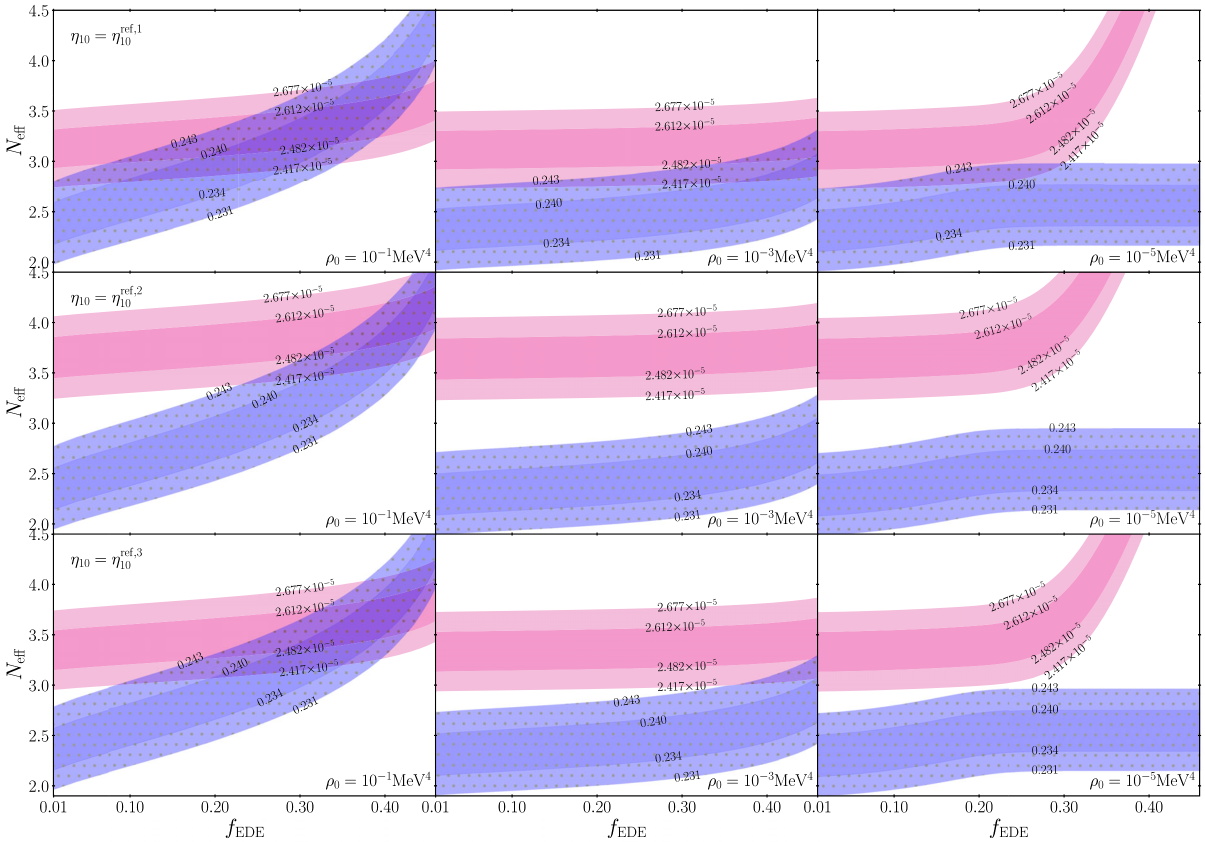

FIG. 10. The same as Fig. 9 except that EDE2 is assumed in this figure.

For the case of EDE1 with the value of ρ_0 shown in the figure, the transition temperature T_t is smaller than 0.07 MeV in most of the range of $f_{\rm EDE}$, and hence the value of Y_p scarcely changes even when $f_{\rm EDE}$ is increased, as explained above. It should also be noticed that $N_{\rm eff}$ has to be smaller than the standard value ($N_{\rm eff} = 3.046$) when $\xi_e = 0$ to satisfy the EMPRESS Y_p value, as seen in the left panel of Fig. 1. Therefore, the allowed region from the Y_p measurement occupies somewhere below $N_{\rm eff} = 3.046$ almost along the horizontal direction to the axis of $f_{\rm EDE}$. Contrary to the behavior of Y_p, the deuterium abundance D_p gets smaller as $f_{\rm EDE}$ increases, and hence the overlapping region appears at some value of $f_{\rm EDE}$, which means that we do not need to assume lepton asymmetry (however, we need a nonstandard value of $N_{\rm eff}$) when the EDE exists. This holds true for all cases of $\eta_{10}^{\rm ref,1}, \eta_{10}^{\rm ref,2}$, and $\eta_{10}^{\rm ref,3}$, although a large fraction of EDE is required when the baryon density is larger (i.e., in the cases of $\eta_{10}^{\rm ref,2}$ and $\eta_{10}^{\rm ref,3}$), which can be noticed by comparing the top and other two lower panels in Fig. 9. When ρ_0 is taken to be small, there is (almost) no overlapping region due to the small contribution from EDE, particularly for the priors of $\eta_{10}^{\rm ref,2}$ and $\eta_{10}^{\rm ref,3}$.

In the case of EDE2 shown in Fig. 10, the responses of D_p and Y_p against the increase of $f_{\rm EDE}$ are opposite to those for EDE1, which were already presented in Fig. 8. However, as in the EDE1 case shown in Fig. 9, the overlapping region between the allowed ones from the Y_p and D_p measurements appears as $f_{\rm EDE}$ increases. It should be noticed that the value of $N_{\rm eff}$ in the overlapping region lies around the standard value for the case of the prior of $\eta_{10} = \eta_{10}^{\rm ref,1}$. This means that the existence of EDE2 can help to fit the EMPRESS Y_p result [9] in combination with the compiled data of D_p [48] without assuming the deviation of $N_{\rm eff}$ from the standard value and with no lepton asymmetry. On the other hand, when a higher baryon density prior such as $\eta_{10} = \eta_{10}^{\rm ref,2}$ and $\eta_{10}^{\rm ref,3}$ is adopted, having an overlapping region becomes a bit difficult, which can be observed from the lower two panels in Fig. 10. Even when such a region exists, the value of $N_{\rm eff}$ is somewhat higher than the standard value. However, we again remark that no lepton asymmetry is assumed in all cases shown in Fig. 10. Thus the EMPRESS Y_p result can be well fitted by assuming the existence of EDE without lepton asymmetry although some nonstandard value for $N_{\rm eff}$ could be required, particularly when the baryon density is high.

To see what values are preferred for the EDE parameters from observations of Y_p and D_p, we show the 1σ and 2σ allowed regions in the $f_{\rm EDE}$-ρ_0 plane for the EDE1 and EDE2 cases in Figs. 11 and 12, respectively. In these figures, we take $\xi_e = 0$ and assume the prior for the baryon

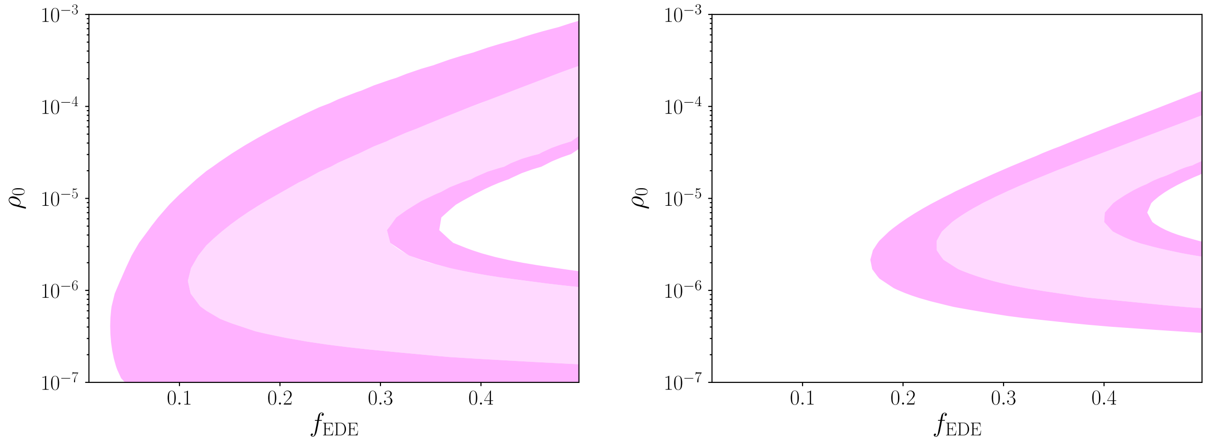

FIG. 11. 1σ and 2σ allowed regions (light and dark shade (magenta), respectively) in the ρ_0-$f_{\rm EDE}$ plane from measurements of Y_p and D_p for EDE1 with $n = 6$ in the cases of $\eta_{10} = \eta_{10}^{\rm ref,1}$ (left) and $\eta_{10}^{\rm ref,2}$ (right). Here we vary $N_{\rm eff}$ and marginalize it. No lepton asymmetry is assumed (i.e., $\xi_e = 0$).

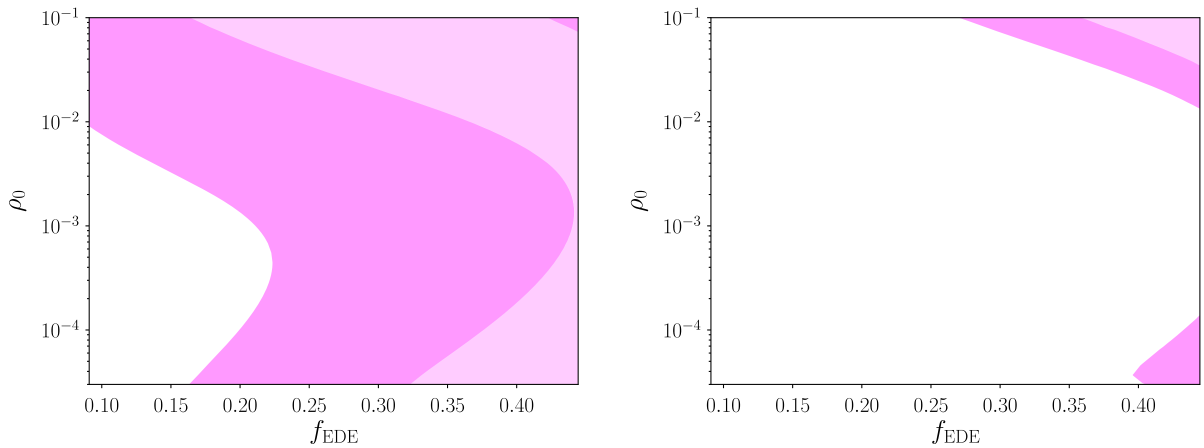

FIG. 12. The same as Fig. 11 but for the case of EDE2.

density as $\eta_{10}^{\rm ref,1}$ (left panel) and $\eta_{10}^{\rm ref,2}$ (right panel). When we adopt the prior of $\eta_{10}^{\rm ref,3}$, we can easily expect that its behavior would be somewhat in between those for $\eta_{10}^{\rm ref,1}$ and $\eta_{10}^{\rm ref,2}$, and hence we do not show such a case here. To obtain the constraints, we vary $N_{\rm eff}$ and marginalize it by choosing the value of $N_{\rm eff}$ that minimizes the value of χ^2 for a given set of $(f_{\rm EDE}, \rho_0)$. As seen from the figures, a nonzero value of $f_{\rm EDE}$ is preferred, which means that the existence of EDE can help to improve the fit. However, for the case of EDE1, although $\xi_e = 0$ can be allowed with the existence of EDE, the value of $N_{\rm eff}$ preferred around the 1σ allowed region in the $f_{\rm EDE}$-ρ_0 plane is $2 \lesssim N_{\rm eff} \lesssim 2.5$ for the priors of both $\eta_{10}^{\rm ref,1}$ and $\eta_{10}^{\rm ref,2}$. On the other hand, for the EDE2 case with the prior of $\eta_{10}^{\rm ref,1}$, the standard value of $N_{\rm eff} \sim 3$ is preferred around the 1σ allowed region, which indicates that the standard scenario with $N_{\rm eff} = 3.046$ and $\xi_e = 0$ can be well allowed with the existence of EDE2. When the prior of $\eta_{10}^{\rm ref,2}$ is adopted for EDE2, a large value for $f_{\rm EDE}$ is preferred, but with an $N_{\rm eff}$ larger than the standard case as $N_{\rm eff} \sim 4$. Even though a nonstandard value for $N_{\rm eff}$ may still be needed in some cases (but with $\xi_e = 0$), Figs. 11 and 12 show that EDE can help to improve the fit to EMPRESS Y_p in combination with D_p.

Next we show constraints from Y_p and D_p in the η_{10}-$N_{\rm eff}$ plane in the presence of EDE with $f_{\rm EDE}$ and ρ_0 being fixed to some values in Fig. 13. The EDE1 and EDE2 cases are, respectively, depicted in left and right panels with $\xi_e = 0$ fixed. For the EDE1 case, we take $f_{\rm EDE} = 0.09$ (magenta) and 0.5 (orange) with $\rho_0 = 10^{-6}$ MeV^4, where light and dark regions, respectively, correspond to the 1σ and 2σ allowed regions. For the EDE2 case, $f_{\rm EDE} = 0.23$ (magenta) and 0.44 (orange) are assumed with $\rho_0 = 10^{-2}$ MeV^4. We fix the EDE parameters $f_{\rm EDE}$ and ρ_0 to show how EDE can improve the fit to Y_p and D_p. For example, in the EDE1 case, when we take $\rho_0 = 10^{-6}$ MeV^4, the existence of EDE can improve the fit depending on the value of $f_{\rm EDE}$. As seen

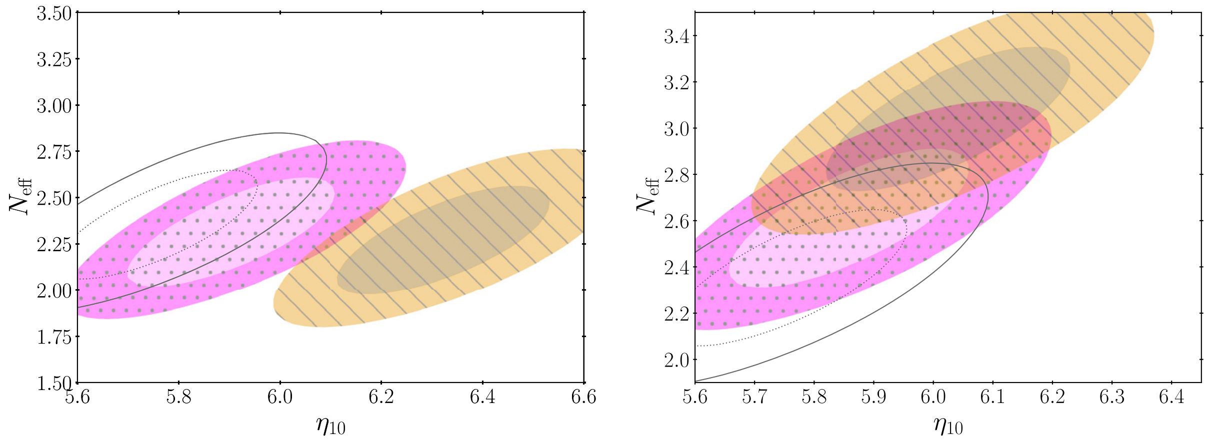

FIG. 13. 1σ and 2σ allowed regions in the η_{10}-N_{eff} plane from measurements of Y_p and D_p for the cases of EDE1 (left) and EDE2 (right). In the left panel, we take $\rho_0 = 10^{-6}$ MeV^4 with $f_{\mathrm{EDE}} = 0.09$ (light and dark dotted (magenta) for 1σ and 2σ regions) and 0.50 (dark and light striped (orange) for 1σ and 2σ regions). In the right panel, we take $\rho_0 = 10^{-2}$ MeV^4 with $f_{\mathrm{EDE}} = 0.23$ (light and dark dotted (magenta) for 1σ and 2σ regions) and 0.44 (dark and light striped (orange) for 1σ and 2σ regions). For reference, we also show the constraint for the case without EDE with black dotted (1σ) and solid (2σ) lines. In both panels, we assume no lepton asymmetry (i.e., $\xi_e = 0$).

in the left panel of Fig. 11, although $f_{\mathrm{EDE}} = 0.09$ corresponds to the parameter near the boundary of the 1σ allowed region, $f_{\mathrm{EDE}} = 0.5$ can give a good fit such that the model is well allowed within 1σ. By comparing these cases, one can see how the EDE parameters affect the constraints in the η_{10}-N_{eff} plane. The choice for the EDE2 case is made in the same spirit.

In the EDE1 case, the deuterium abundance is more affected than Y_p, and hence the effect of f_{EDE} degenerates with that of the baryon density since D_p is sensitive to the change of η_{10}. Therefore, as f_{EDE} increases, the allowed region shifts almost horizontally to the right. As discussed in the previous section, when the baryon density is suggested to take a larger value, N_{eff} needs to be larger than the standard case and ξ_e should be (positively) nonzero when no EDE is assumed (see Fig. 1). However, when EDE is present, as the fraction of EDE increases, the allowed region is shifted to a higher value of η_{10}, although N_{eff} needs to be smaller than the standard value of $N_{\mathrm{eff}} = 3.046$. Even if the H_0 tension really demands that we need a high value for η_{10}, the EDE1 model can reduce the discrepancy of the baryon density between the EMPRESS Y_p result and CMB data with a low value for N_{eff}.

In the case of EDE2, the value of Y_p is decreased by taking a larger value for f_{EDE}, which can cancel the increase of Y_p resulting from a larger value for N_{eff}. Therefore, by appropriately choosing the values of f_{EDE} and ρ_0, the EDE model can well fit the EMPRESS Y_p [9] and D_p result from Ref. [26] simultaneously with the standard value of N_{eff} and without assuming lepton asymmetry when the baryon density is $\eta_{10} \sim 6.14$, which was obtained from the *Planck* data in the framework of ΛCDM. However, when a higher baryon density is suggested from CMB data, which could be motivated in light of the H_0 tension, one needs a larger value for N_{eff} than the standard one. When $\eta_{10} \sim 6.4$, the EDE2 model with $f_{\mathrm{EDE}} = 0.44$ and $\rho_0 = 8 \times 10^{-2}$ MeV^4 can be well fitted to the data, but with $N_{\mathrm{eff}} = 4.0$. In any case, the existence of EDE can help to improve the fit to the EMPRESS Y_p result without resorting to lepton asymmetry even if a higher baryon density is suggested.

Finally, we discuss constraints in the N_{eff}-ξ_e plane. The 1σ and 2σ allowed regions are shown for the cases of EDE1 and EDE2 in Figs. 14 and 15, respectively. In each figure, two priors for η_{10}, i.e., $\eta_{10} = \eta_{10}^{\mathrm{ref},1} \pm \sigma_{\eta_{10},1}$ and $\eta_{10}^{\mathrm{ref},2} \pm \sigma_{\eta_{10},2}$, are adopted, which are, respectively, shown in left and right panels in the figures. In these figures, we fix the EDE parameters f_{EDE} and ρ_0 to some specific values, whose actual values are chosen in the same spirit as the one for Fig. 13, which has already been mentioned above. For reference, we also show the constraints for the case without EDE.

In the case of EDE1 shown in Fig. 14, we take $f_{\mathrm{EDE}} = 0.09$ (magenta) and 0.44 (orange) with $\rho_0 = 10^{-6}$ MeV^4, where light and dark regions correspond to the 1σ and 2σ allowed regions, respectively. Since a larger f_{EDE} gives larger Y_p and D_p, the decreases of N_{eff} and ξ_e are canceled by a large value of f_{EDE} and hence the allowed region shifts to the one with smaller N_{eff} and smaller ξ_e by increasing f_{EDE}. Although the standard point with $N_{\mathrm{eff}} = 3.046$ and $\xi_e = 0$ is a bit away from the 2σ bound for the priors of both $\eta_{10}^{\mathrm{ref},1}$ and $\eta_{10}^{\mathrm{ref},2}$, either $N_{\mathrm{eff}} = 3.046$ or $\xi_e = 0$ can be realized by appropriately choosing the values of f_{EDE} and ρ_0 in the EDE1 case. Notice that this holds true even if the prior of a large baryon density $\eta_{10}^{\mathrm{ref},2}$ is adopted where a

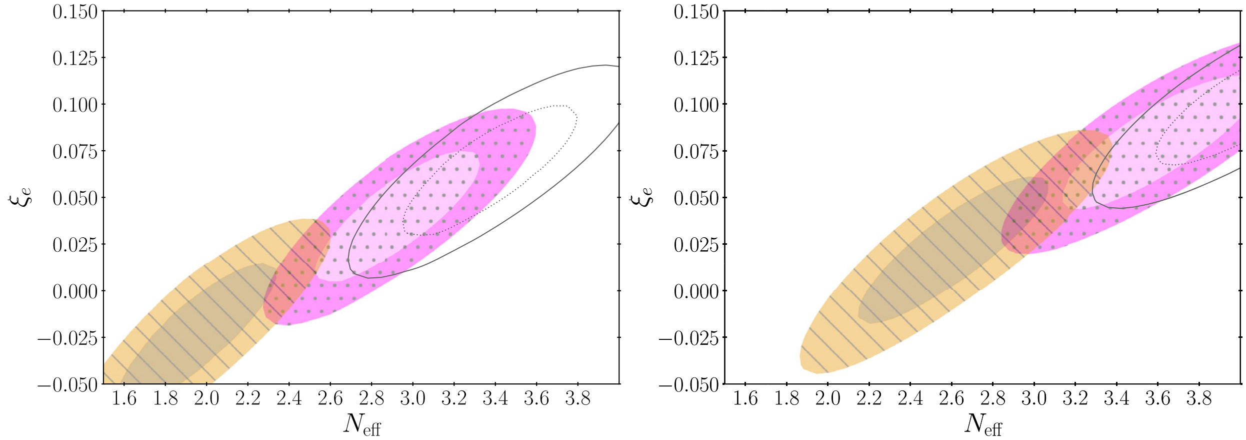

FIG. 14. 1σ and 2σ allowed regions in the $N_{\rm eff}$-ξ_e plane for the case with EDE1, adopting the priors of $\eta_{10} = \eta_{10}^{\rm ref,1} \pm \sigma_{\eta_{10},1}$ (left) and $\eta_{10} = \eta_{10}^{\rm ref,2} \pm \sigma_{\eta_{10},2}$ (right). We take $f_{\rm EDE} = 0.09$ (light and dark dotted (magenta) for 1σ and 2σ regions) and 0.44 (dark and light striped (orange) for 1σ and 2σ regions) with $\rho_0 = 10^{-6}$ MeV^4. For reference, we also show the constraint for the case without EDE with black dotted (1σ) and solid (2σ) lines.

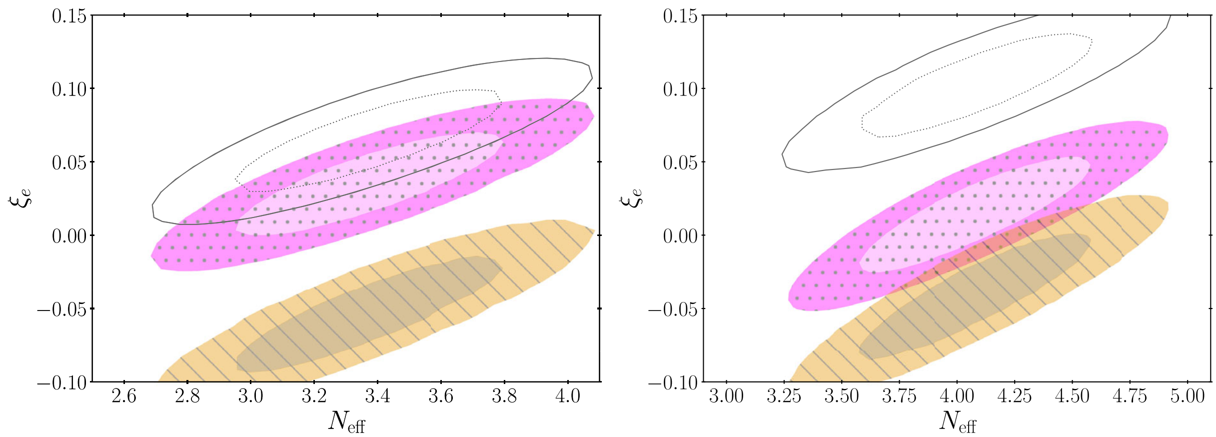

FIG. 15. 1σ and 2σ allowed regions in the $N_{\rm eff}$-ξ_e plane for the case with the EDE2, adopting the priors of $\eta_{10} = \eta_{10}^{\rm ref,1} \pm \sigma_{\eta_{10},1}$ (left) and $\eta_{10} = \eta_{10}^{\rm ref,2} \pm \sigma_{\eta_{10},2}$ (right). In the left panel, we take $f_{\rm EDE} = 0.17$ (light and dark dotted (magenta) for 1σ and 2σ regions) and 0.44 (dark and light striped (orange) for 1σ and 2σ regions). In the right panel, we take $f_{\rm EDE} = 0.41$ (light and dark dotted (magenta) for 1σ and 2σ regions) and 0.47 (dark and light striped (orange) for 1σ and 2σ regions). In both panels, ρ_0 is assumed as $\rho_0 = 10^{-1}$ MeV^4. For reference, we also show the constraint for the case without EDE with black dotted (1σ) and solid (2σ) lines.

greater deviation from the standard values for both $N_{\rm eff}$ and ξ_e is required to fit the EMPRESS Y_p result without EDE.

In the case of EDE2, depicted in Fig. 15, we assume $f_{\rm EDE} = 0.17$ (magenta) and 0.44 (orange) in the left panel. In the right panel, $f_{\rm EDE} = 0.41$ (magenta) and 0.47 (orange) are assumed. In both panels, we take $\rho_0 = 10^{-1}$ MeV^4. As can be noticed from the figure, by changing the values of $f_{\rm EDE}$ and ρ_0, the allowed region in the $N_{\rm eff}$-ξ_e plane moves almost vertically downwards. One can see that, when the baryon density is $\eta_{10} \sim 6.14$, the standard value of $N_{\rm eff}$ with no lepton asymmetry can be well fitted to the EMPRESS Y_p result in the presence of EDE with appropriately chosen $f_{\rm EDE}$ and ρ_0. On the other hand, when a high baryon density prior of $\eta_{10}^{\rm ref,2}$ is adopted, the EMPRESS result demands a value of $N_{\rm eff}$ higher than the standard one, even assuming the presence of EDE. However, it should be emphasized that both a high value of $N_{\rm eff}$ and a positively nonzero ξ_e are required to fit the EMPRESS Y_p result when EDE is absent, which can be seen from the right panel of Fig. 2; on the other hand, once we assume EDE, one can fit the EMPRESS Y_p without any lepton asymmetry, which indicates that EDE can mitigate the helium anomaly caused by the EMPRESS Y_p results.

IV. CONCLUSION AND DISCUSSION

In this paper, we first investigated the impact of the H_0 tension, in which a higher value for the baryon density than that in the ΛCDM framework could be preferred, on BBN in light of recent Y_p measurement by EMPRESS. As already pointed out [9], the EMPRESS Y_p result would infer a value of $N_{\rm eff}$ higher than the standard case and a positively nonzero value of ξ_e. However, given that models proposed to resolve the H_0 tension tend to prefer a higher baryon density than that in the ΛCDM model adopted in Ref. [9], the deviation from the standard assumption ($N_{\rm eff} = 3.046$ and $\xi_e = 0$) would be more significant. As shown in Figs. 1 and 2, when a large η_{10} is assumed, which is suggested by the H_0 tension, $N_{\rm eff}$ needs to be much larger than the standard value of $N_{\rm eff} = 3.046$ and ξ_e should take a large positively nonzero value to explain the EMPRESS Y_p value in combination with the D_p measurement of Ref. [26]. Therefore, the H_0 tension could also affect BBN, which shows that the tension would have a further impact on other aspects of cosmology.

We also studied the effects of early dark energy, which has been extensively investigated in the context of the H_0 tension, on the abundances of helium and deuterium. As mentioned above, the EMPRESS Y_p results suggest that nonstandard values of $N_{\rm eff}$ and a nonzero ξ_e are necessary to have a good fit to Y_p and D_p data simultaneously; however, by assuming the existence of early dark energy which takes a sizable fraction in the total energy density during BBN, the values of $N_{\rm eff}$ and ξ_e can still take the standard values, depending on the EDE model and parameters. Even if a larger value of η_{10} is assumed, which could be demanded by models resolving the H_0 tension, the existence of early dark energy can still reduce the tension such that $N_{\rm eff}$ and ξ_e can take values close to the standard ones. Therefore, early dark energy can improve the fit even in the case of a large baryon density in light of the EMPRESS Y_p results.

The recent EMPRESS results may suggest physics beyond the standard cosmological model. By taking account of the H_0 tension, which is one of the most significant tensions in cosmology today, more modification and extension to the standard model would be required. Our study may indicate that the tensions in cosmology should be simultaneously investigated in order to pursue a new cosmological model, from which one can gain profound insight into not only the evolution of the Universe, but also the fundamental law of physics.

ACKNOWLEDGMENTS

The work of T. T. was supported by JSPS KAKENHI Grant Number 19K03874.

[1] A. G. Riess *et al.*, A comprehensive measurement of the local value of the Hubble constant with 1 km/s/Mpc uncertainty from the Hubble space telescope and the SH0ES team, Astrophys. J. Lett. **934**, L7 (2022).

[2] N. Aghanim *et al.* (Planck Collaboration), Planck 2018 results. VI. Cosmological parameters, Astron. Astrophys. **641**, A6 (2020); **652**, C4(E) (2021).

[3] N. Schöneberg, J. Lesgourgues, and D. C. Hooper, The BAO + BBN take on the Hubble tension, J. Cosmol. Astropart. Phys. 10 (2019) 029.

[4] F. Okamatsu, T. Sekiguchi, and T. Takahashi, H_0 tension without CMB data: Beyond the ΛCDM, Phys. Rev. D **104**, 023523 (2021).

[5] N. Schöneberg, L. Verde, H. Gil-Marín, and S. Brieden, BAO+BBN revisited—Growing the Hubble tension with a 0.7 km/s/Mpc constraint, J. Cosmol. Astropart. Phys. 11 (2022) 039.

[6] E. Di Valentino, O. Mena, S. Pan, L. Visinelli, W. Yang, A. Melchiorri, D. F. Mota, A. G. Riess, and J. Silk, In the realm of the Hubble tension—a review of solutions, Classical Quantum Gravity **38**, 153001 (2021).

[7] L. Perivolaropoulos and F. Skara, Challenges for ΛCDM: An update, New Astron. Rev. **95**, 101659 (2022).

[8] N. Schöneberg, G. Franco Abellán, A. Pérez Sánchez, S. J. Witte, V. Poulin, and J. Lesgourgues, The H0 Olympics: A fair ranking of proposed models, Phys. Rep. **984**, 1 (2022).

[9] A. Matsumoto *et al.*, EMPRESS. VIII. A new determination of primordial He abundance with extremely metal-poor galaxies: A suggestion of the lepton asymmetry and implications for the Hubble tension, Astrophys. J. **941**, 167 (2022).

[10] E. Aver, K. A. Olive, and E. D. Skillman, The effects of He I λ10830 on helium abundance determinations, J. Cosmol. Astropart. Phys. 07 (2015) 011.

[11] T. Hsyu, R. J. Cooke, J. X. Prochaska, and M. Bolte, The PHLEK survey: A new determination of the primordial helium abundance, Astrophys. J. **896**, 77 (2020).

[12] O. A. Kurichin, P. A. Kislitsyn, V. V. Klimenko, S. A. Balashev, and A. V. Ivanchik, A new determination of the primordial helium abundance using the analyses of H II region spectra from SDSS, Mon. Not. R. Astron. Soc. **502**, 3045 (2021).

[13] R. J. Cooke, M. Pettini, and C. C. Steidel, One percent determination of the primordial deuterium abundance, Astrophys. J. **855**, 102 (2018).

[14] G. Mangano, G. Miele, S. Pastor, T. Pinto, O. Pisanti, and P. D. Serpico, Relic neutrino decoupling including flavor oscillations, Nucl. Phys. **B729**, 221 (2005).

[15] P. F. de Salas and S. Pastor, Relic neutrino decoupling with flavour oscillations revisited, J. Cosmol. Astropart. Phys. 07 (2016) 051.

[16] M. Escudero Abenza, Precision early universe thermodynamics made simple: $N_{\rm eff}$ and neutrino decoupling in the

Standard Model and beyond, J. Cosmol. Astropart. Phys. 05 (2020) 048.

[17] K. Akita and M. Yamaguchi, A precision calculation of relic neutrino decoupling, J. Cosmol. Astropart. Phys. 08 (2020) 012.

[18] J. Froustey, C. Pitrou, and M. C. Volpe, Neutrino decoupling including flavour oscillations and primordial nucleosynthesis, J. Cosmol. Astropart. Phys. 12 (2020) 015.

[19] J. J. Bennett, G. Buldgen, P. F. De Salas, M. Drewes, S. Gariazzo, S. Pastor, and Y. Y. Y. Wong, Towards a precision calculation of $N_{\rm eff}$ in the Standard Model II: Neutrino decoupling in the presence of flavour oscillations and finite-temperature QED, J. Cosmol. Astropart. Phys. 04 (2021) 073.

[20] O. Seto and Y. Toda, Hubble tension in lepton asymmetric cosmology with an extra radiation, Phys. Rev. D **104**, 063019 (2021).

[21] M. Kawasaki and K. Murai, Lepton asymmetric universe, J. Cosmol. Astropart. Phys. 08 (2022) 041.

[22] A.-K. Burns, T. M. P. Tait, and M. Valli, Indications for a Nonzero Lepton Asymmetry in the Early Universe, Phys. Rev. Lett. **130**, 131001 (2023).

[23] D. Borah and A. Dasgupta, Large neutrino asymmetry from TeV scale leptogenesis in the light of helium anomaly, arXiv:2206.14722.

[24] M. Escudero, A. Ibarra, and V. Maura, Primordial lepton asymmetries in the precision cosmology era: Current status and future sensitivities from BBN and the CMB, Phys. Rev. D **107**, 035024 (2023).

[25] K. Kohri and K.-i. Maeda, A possible solution to the helium anomaly of EMPRESS VIII by cuscuton gravity theory, Prog. Theor. Exp. Phys. **2022**, 091E01 (2022).

[26] R. L. Workman *et al.* (Particle Data Group Collaboration), Review of particle physics, Prog. Theor. Exp. Phys. **2022**, 083C01 (2022).

[27] V. Poulin, T. L. Smith, T. Karwal, and M. Kamionkowski, Early Dark Energy Can Resolve The Hubble Tension, Phys. Rev. Lett. **122**, 221301 (2019).

[28] T. Sekiguchi and T. Takahashi, Cosmological bound on neutrino masses in the light of H_0 tension, Phys. Rev. D **103**, 083516 (2021).

[29] G. Ye, B. Hu, and Y.-S. Piao, Implication of the Hubble tension for the primordial Universe in light of recent cosmological data, Phys. Rev. D **104**, 063510 (2021).

[30] F. Takahashi and W. Yin, Cosmological implications of $n_s \approx 1$ in light of the Hubble tension, Phys. Lett. B **830**, 137143 (2022).

[31] J.-Q. Jiang and Y.-S. Piao, Toward early dark energy and ns = 1 with Planck, ACT, and SPT observations, Phys. Rev. D **105**, 103514 (2022).

[32] G. Ye, J.-Q. Jiang, and Y.-S. Piao, Towards hybrid inflation with $n_s = 1$ in light of Hubble tension and primordial gravitational waves, Phys. Rev. D **106**, 103528 (2022).

[33] T. Sekiguchi and T. Takahashi, Early recombination as a solution to the H_0 tension, Phys. Rev. D **103**, 083507 (2021).

[34] G. Ye and Y.-S. Piao, Is the Hubble tension a hint of AdS phase around recombination?, Phys. Rev. D **101**, 083507 (2020).

[35] J. C. Hill, E. McDonough, M. W. Toomey, and S. Alexander, Early dark energy does not restore cosmological concordance, Phys. Rev. D **102**, 043507 (2020).

[36] F. Niedermann and M. S. Sloth, Resolving the Hubble tension with new early dark energy, Phys. Rev. D **102**, 063527 (2020).

[37] M. Braglia, M. Ballardini, F. Finelli, and K. Koyama, Early modified gravity in light of the H_0 tension and LSS data, Phys. Rev. D **103**, 043528 (2021).

[38] K. Jedamzik and L. Pogosian, Relieving the Hubble Tension with Primordial Magnetic Fields, Phys. Rev. Lett. **125**, 181302 (2020).

[39] M. Escudero and S. J. Witte, The Hubble tension as a hint of leptogenesis and neutrino mass generation, Eur. Phys. J. C **81**, 515 (2021).

[40] K. Ichikawa, T. Sekiguchi, and T. Takahashi, Primordial helium abundance from CMB: A constraint from recent observations and a forecast, Phys. Rev. D **78**, 043509 (2008).

[41] K. Ichikawa, T. Sekiguchi, and T. Takahashi, Probing the effective number of neutrino species with cosmic microwave background, Phys. Rev. D **78**, 083526 (2008).

[42] R. Consiglio, P. F. de Salas, G. Mangano, G. Miele, S. Pastor, and O. Pisanti, PArthENoPE reloaded, Comput. Phys. Commun. **233**, 237 (2018).

[43] P. D. Serpico, S. Esposito, F. Iocco, G. Mangano, G. Miele, and O. Pisanti, Nuclear reaction network for primordial nucleosynthesis: A detailed analysis of rates, uncertainties and light nuclei yields, J. Cosmol. Astropart. Phys. 12 (2004) 010.

[44] G. Steigman, The cosmological evolution of the average mass per baryon, J. Cosmol. Astropart. Phys. 10 (2006) 016.

[45] O. Pisanti, A. Cirillo, S. Esposito, F. Iocco, G. Mangano, G. Miele, and P. D. Serpico, PArthENoPE: Public algorithm evaluating the nucleosynthesis of primordial elements, Comput. Phys. Commun. **178**, 956 (2008).

[46] S. Gariazzo, P. F. de Salas, O. Pisanti, and R. Consiglio, PArthENoPE revolutions, Comput. Phys. Commun. **271**, 108205 (2022).

[47] K. Kohri, M. Kawasaki, and K. Sato, Big bang nucleosynthesis and lepton number asymmetry in the universe, Astrophys. J. **490**, 72 (1997).

[48] P. A. Zyla *et al.* (Particle Data Group Collaboration), Review of particle physics, Prog. Theor. Exp. Phys. **2020**, 083C01 (2020).

[49] J. P. Kneller and G. Steigman, BBN for pedestrians, New J. Phys. **6**, 117 (2004).

[50] M. Kamionkowski, J. Pradler, and D. G. E. Walker, Dark Energy from the String Axiverse, Phys. Rev. Lett. **113**, 251302 (2014).

[51] K. Freese and M. W. Winkler, Chain early dark energy: A Proposal for solving the Hubble tension and explaining today's dark energy, Phys. Rev. D **104**, 083533 (2021).

[52] K. Rezazadeh, A. Ashoorioon, and D. Grin, Cascading dark energy, arXiv:2208.07631.

[53] E. Mörtsell and S. Dhawan, Does the Hubble constant tension call for new physics?, J. Cosmol. Astropart. Phys. 09 (2018) 025.

[54] V. Poulin, K. K. Boddy, S. Bird, and M. Kamionkowski, Implications of an extended dark energy cosmology with massive neutrinos for cosmological tensions, Phys. Rev. D **97**, 123504 (2018).

[55] T. Delubac *et al.* (BOSS Collaboration), Baryon acoustic oscillations in the Lyα forest of BOSS DR11 quasars, Astron. Astrophys. **574**, A59 (2015).

[56] E. Aubourg *et al.*, Cosmological implications of baryon acoustic oscillation measurements, Phys. Rev. D **92**, 123516 (2015).

[57] H. du Mas des Bourboux *et al.*, Baryon acoustic oscillations from the complete SDSS-III Lyα-quasar cross-correlation function at $z = 2.4$, Astron. Astrophys. **608**, A130 (2017).

[58] H. du Mas des Bourboux *et al.*, The completed SDSS-IV extended baryon oscillation spectroscopic survey: Baryon acoustic oscillations with Lyα forests, Astrophys. J. **901**, 153 (2020).

[59] Y. Wang, L. Pogosian, G.-B. Zhao, and A. Zucca, Evolution of dark energy reconstructed from the latest observations, Astrophys. J. Lett. **869**, L8 (2018).

[60] K. Dutta, Ruchika, A. Roy, A. A. Sen, and M. M. Sheikh-Jabbari, Beyond ΛCDM with low and high redshift data: Implications for dark energy, Gen. Relativ. Gravit. **52**, 15 (2020).

[61] M. Fasiello and A. J. Tolley, Cosmological stability bound in massive gravity and bigravity, J. Cosmol. Astropart. Phys. 12 (2013) 002.

[62] Y. Akrami, S. F. Hassan, F. Könnig, A. Schmidt-May, and A. R. Solomon, Bimetric gravity is cosmologically viable, Phys. Lett. B **748**, 37 (2015).

[63] F. Könnig, Higuchi ghosts and gradient instabilities in bimetric gravity, Phys. Rev. D **91**, 104019 (2015).

[64] O. Akarsu, J. D. Barrow, L. A. Escamilla, and J. A. Vazquez, Graduated dark energy: Observational hints of a spontaneous sign switch in the cosmological constant, Phys. Rev. D **101**, 063528 (2020).

[65] O. Akarsu, S. Kumar, E. Özülker, and J. A. Vazquez, Relaxing cosmological tensions with a sign switching cosmological constant, Phys. Rev. D **104**, 123512 (2021).

[66] O. Akarsu, S. Kumar, E. Ozulker, J. A. Vazquez, and A. Yadav, Relaxing cosmological tensions with a sign switching cosmological constant: Improved results with Planck, BAO and Pantheon data, arXiv:2211.05742.

[67] M. Ahmed, S. Dodelson, P. B. Greene, and R. Sorkin, Everpresent Λ, Phys. Rev. D **69**, 103523 (2004).

[68] N. Zwane, N. Afshordi, and R. D. Sorkin, Cosmological tests of Everpresent Λ, Classical Quantum Gravity **35**, 194002 (2018).